

$Hb\bar{b}$ production in Composite Higgs Models

Mikael Chala and José Santiago

*CAFPE and Departamento de Física Teórica y del Cosmos,
Universidad de Granada, E-18071 Granada, Spain*

Abstract

New vector-like quarks with electric charge $2/3$ and $-1/3$ can be singly produced at hadron colliders through the exchange of a color octet vector resonance in models of strong electroweak symmetry breaking. We show that electroweak symmetry breaking effects can have a significant impact on the decay pattern of these new quarks. In particular, single production of charge $-1/3$ fermion resonances, mediated by a color octet vector resonance, typically results in an $Hb\bar{b}$ final state with a sizeable cross section and very distinctive kinematics. We consider the leading $H \rightarrow b\bar{b}$ decay and show that the $4b$ signal can be very efficiently disentangled from the background: heavy octet masses of up to 3 TeV can be tested with the data already collected at the LHC and up to 5 TeV with an integrated luminosity of 100 fb^{-1} at $\sqrt{s} = 14 \text{ TeV}$. We also discuss the kinematical differences between the $Hb\bar{b}$ production in models of strong electroweak symmetry breaking and supersymmetric models and the implications on the phenomenology of non-minimal composite Higgs models.

I. INTRODUCTION

Composite Higgs models are among the leading candidates to dynamically explain the origin of the electroweak symmetry breaking (EWSB) scale. The absence of any significant departure from the Standard Model (SM) predictions in current LHC searches, although somewhat disappointing, was not unexpected [1]. The reason is that the constraints that electroweak precision tests typically impose on the scale of the new resonances are stringent enough to make their discovery in the low energy phase of the LHC highly unlikely. New vector resonances are expected to have masses in the multi-TeV range, well above the current LHC reach [2–4]. Naturalness [5–9] and compatibility with electroweak precision tests [10–12] on the other hand predict fermion resonances to be relatively light with typical masses below the TeV scale.

These new fermion resonances, called top partners, are vector-like quarks that mix strongly with the SM top quark. They are arranged in multiplets of the unbroken global symmetries of the composite sector which are likely to include at the very least an $SO(4)$ custodial symmetry. Top partners can be efficiently searched for at the LHC through their pair or single (electroweak) production [13–18] and current data are already starting to probe part of the region of parameter space allowed by indirect constraints. It has been recently pointed out that top partners can be also singly produced via the s-channel exchange of a color octet vector resonance. This production mechanism can be competitive with the previous ones and has the advantage of probing different aspects of the composite sector [19–21]. Note that, even if *a priori* the composite sector does not need to have color octet vector resonances, they naturally occur in models in which partial compositeness [22, 23] is realized.

In this article we will show that if the bottom partners, the fermion resonances responsible for the mass of the bottom quark, are not much heavier than the top partners there can be a sizeable production of $Hb\bar{b}$ events in composite Higgs models [24]. The large cross section has its origin in the single production of a bottom

partner, via the s-channel exchange of a heavy color octet vector, followed by the decay into a Higgs boson and the SM bottom quark:

$$pp \rightarrow G^* \rightarrow B_H \bar{b} + b \bar{B}_H \rightarrow H b \bar{b}, \quad (1)$$

where we have denoted by G^* the vector resonance, called from now on heavy gluon, and B_H the bottom partner (heavy bottom). If flavor is realized through partial compositeness the bottom quark is lighter than the top quark because it is less composite and not because its partners are much heavier. EWSB effects, on the other hand, are quite relevant to correctly describe the phenomenology of bottom partners. Due to the small mixing between the bottom quark and its partners, the presence of other fermion resonances and the sizeable Yukawa couplings among them can have a large impact in the decay pattern of the heavy fermions. We explain the origin of this effect and its possible relevance in models of strong EWSB in Appendix A. In the example described in the appendix the only resonance accessible at the LHC is the partner of the b_R but it has a phenomenology wildly different from a vector-like singlet. This shows that when large couplings are expected among the new particles -like in models of strong EWSB- heavier states beyond the LHC reach can have a huge impact on the phenomenology of the lighter resonances that we can access experimentally. Thus we see that simplified models which consider only the lightest resonances in the spectrum, although an interesting first approach to models of new physics, can have a phenomenology that grossly deviates from the actual phenomenology of the full models.

$H b \bar{b}$ production with $H \rightarrow b \bar{b}$ decay has been proposed as a useful channel to search for neutral scalars in supersymmetric models at large $\tan \beta$ [25–28]. The $\tan \beta$ enhancement of the cross section is however dwarfed by the huge QCD background and the difficulty of a clean trigger (imposing a hard cut on the p_T of all four b jets reduces the signal to negligible levels). In our case, the large masses of the intermediate particles (G^* and B_H) change the picture completely. We can impose very stringent cuts on the p_T of the b jets, which ensure a clean triggering and a very

efficient reduction of the background. We will show that the specific kinematics of the process allows for an excellent reconstruction of both the bottom partner and the heavy gluon. Other searches that are sensitive to the signature we study in this article, again motivated by supersymmetric models, involve final states with a large number of b -jets plus a sizeable amount of missing energy. Our signal does not have real missing energy but the large energy of the quarks involved represent a non-negligible source of fake missing E_T . We will show that simple modifications of current multi- b searches, like the requirement of harder b -jets and/or less missing energy, can turn these analyses into very powerful probes of composite Higgs models.

The main results of this work are the expected 95% C.L. exclusion bounds on the single production cross section of B_H (via a heavy gluon) times its branching fraction into $Hb\bar{b}$ and the discovery reach, that we report as a function of the main parameters of the model. We have found that, assuming $M_B \approx M_{G^*}/2$, masses up to ~ 3 (2.75) TeV for the heavy gluon can be excluded (discovered) with the data already collected at the LHC. This extends up to ~ 5 and 4.5 TeV of exclusion and discovery limits for the LHC with $\sqrt{s} = 14$ TeV and an integrated luminosity of 100 fb^{-1} .

Finally, we will argue that in composite Higgs models with an extended scalar sector [29–34], a similar process in which the Higgs boson is replaced by a mostly singlet composite scalar might be the discovery mode for these scalars.

This article is organized as follows: we describe our model in Section II. The most relevant features of the $Hb\bar{b}$ production mechanism in composite Higgs models are discussed in Section III. We then introduce the experimental analysis to search for this signature at the LHC. We discuss our results, given in terms of exclusion bounds and discovery limits in section V and we leave our conclusions for section VI. We describe in Appendix A some technical aspects of the model, including the importance of EWSB effects in the phenomenology of the lightest fermionic resonances and give an example of the slow decoupling of heavy partners in models of strong EWSB. The relevance of $4b$ final states as a discovery channel for mostly singlet

composite scalars is discussed in Appendix B.

II. THE MODEL

We consider a simplified, two-site [20] version of the minimal composite Higgs model [2, 35, 36] that contains a full description of the bottom sector. This model captures the mechanism of partial compositeness and the implications of the global symmetries in the composite sector. For clarity we neglect non-linear Higgs couplings due to its pseudo-Nambu-Goldstone nature (see [17, 37, 38] for a discussion of the corresponding effects). In this section we will describe the main relevant features of the model. Further details can be found in [20].

The model consists of a composite sector, with a global $SU(3)_c \times SU(2)_L \times SU(2)_R \times U(1)_X$ symmetry plus a P_{LR} parity that exchanges $SU(2)_L$ and $SU(2)_R$, and an elementary sector, which contains the SM particles minus the Higgs. Among the composite resonances, the ones that will play a role in the following are a color octet vector, G^c , transforming in the $(\mathbf{8}, \mathbf{1}, \mathbf{1})_0$ representation of the global symmetry, the composite Higgs

$$\mathcal{H} = (\mathbf{1}, \mathbf{2}, \mathbf{2})_0 = \begin{bmatrix} \phi_0^\dagger & \phi^+ \\ -\phi^- & \phi_0 \end{bmatrix}, \quad (2)$$

and the top and bottom partners

$$\mathcal{Q} = (\mathbf{3}, \mathbf{2}, \mathbf{2})_{2/3} = \begin{bmatrix} T^c & T_{5/3}^c \\ B^c & T_{2/3}^c \end{bmatrix}, \quad \tilde{T}^c = (\mathbf{3}, \mathbf{1}, \mathbf{1})_{2/3}, \quad (3)$$

$$\mathcal{Q}' = (\mathbf{3}, \mathbf{2}, \mathbf{2})_{-1/3} = \begin{bmatrix} B_{-1/3}^c & T'^c \\ B_{-4/3}^c & B'^c \end{bmatrix}, \quad \tilde{B}^c = (\mathbf{3}, \mathbf{1}, \mathbf{1})_{-1/3}. \quad (4)$$

The subscript in the name of the quark denotes its electric charge, given by $Q = T_3^L + Y = T_3^L + T_3^R + X$, with X the charge under the $U(1)_X$ group. Among the quarks with no subscript, T^c , \tilde{T}^c and T'^c have electric charge $2/3$ and B^c , B'^c and \tilde{B}^c have electric charge $-1/3$. Finally, the superscript c is a reminder that they belong to the composite sector.

The Lagrangian involving these fields reads

$$\begin{aligned}
\mathcal{L} = & -\frac{1}{2}\text{Tr}[G_{\mu\nu}^e G^{e\mu\nu}] + \frac{1}{2}\left(\frac{g_e M_{G^c}}{g_c}\right)^2 (G_\mu^e)^2 + \bar{q}_L^e i\not{D}q_L^e + \bar{t}_R^e i\not{D}t_R^e + \bar{b}_R^e i\not{D}b_R^e \\
& -\frac{1}{2}\text{Tr}[G_{\mu\nu}^c G^{c\mu\nu}] + \frac{1}{2}M_{G^c}^2 (G_\mu^c)^2 + \frac{1}{2}\text{Tr}[\partial_\mu \mathcal{H}^\dagger \partial^\mu \mathcal{H}] - V(\mathcal{H}^\dagger \mathcal{H}) \\
& + \text{Tr}[\bar{\mathcal{Q}}(i\not{\partial} - g_c \mathcal{G}^c - M_{\mathcal{Q}})\mathcal{Q}] + \bar{T}^c(i\not{\partial} - g_c \mathcal{G}^c - M_{\tilde{T}^c})\tilde{T}^c \\
& + \text{Tr}[\bar{\mathcal{Q}}'(i\not{\partial} - g_c \mathcal{G}^c - M_{\mathcal{Q}'})\mathcal{Q}'] + \bar{B}^c(i\not{\partial} - g_c \mathcal{G}^c - M_{\tilde{B}^c})\tilde{B}^c \\
& - \left\{ Y_T \text{Tr}[\bar{\mathcal{Q}}\mathcal{H}]\tilde{T} + Y_B \text{Tr}[\bar{\mathcal{Q}}'\mathcal{H}]\tilde{B} \right. \\
& + \frac{1}{2}\frac{g_e}{g_c} M_{G^c}^2 G_\mu^c G^{e\mu} + \Delta_{L1} \bar{q}_L^e (T^c, B^e)^T + \Delta_{L2} \bar{q}_L^e (T'^c, B'^e)^T \\
& \left. + \Delta_{tR} \bar{t}_R^e \tilde{T}^c + \Delta_{bR} \bar{b}_R^e \tilde{B}^c + \text{h.c.} \right\} + \dots . \tag{5}
\end{aligned}$$

The first line involves only elementary fields (denoted with a superscript e), the next four only composite states and the last two the linear mixing among the two sectors realizing partial compositeness. This linear mixing can be eliminated by performing the appropriate rotations so that the physical particles (before EWSB) are an admixture of elementary and composite states. For instance we can define the physical SM gluon and heavy gluon as follows:

$$\begin{pmatrix} G_\mu \\ G_\mu^* \end{pmatrix} = \begin{pmatrix} c_s & s_s \\ -s_s & c_s \end{pmatrix} \begin{pmatrix} G_\mu^e \\ G_\mu^c \end{pmatrix}, \tag{6}$$

with $s_s/c_s \equiv \sin\theta_s/\cos\theta_s = g_e/g_c$. The SM gluon is of course massless and has a coupling $g_s = s_s g_c = c_s g_e$ and the heavy gluon has a mass $M_{G^*} = M_{G^c}/c_s$ and coupling $-g_s s_s/c_s$ to elementary states and $g_s c_s/s_s$ to composite ones. In a similar way we can define the SM t_R and b_R and the heavy vector-like singlets \tilde{T} and \tilde{B} ,

$$\begin{pmatrix} t_R \\ \tilde{T}_R \end{pmatrix} = \begin{pmatrix} c_{tR} & -s_{tR} \\ s_{tR} & c_{tR} \end{pmatrix} \begin{pmatrix} t_R^e \\ \tilde{T}_R^c \end{pmatrix}, \quad \tilde{T}_L = \tilde{T}_L^c, \tag{7}$$

$$\begin{pmatrix} b_R \\ \tilde{B}_R \end{pmatrix} = \begin{pmatrix} c_{bR} & -s_{bR} \\ s_{bR} & c_{bR} \end{pmatrix} \begin{pmatrix} b_R^e \\ \tilde{B}_R^c \end{pmatrix}, \quad \tilde{B}_L = \tilde{B}_L^c. \tag{8}$$

with

$$\frac{s_{tR}}{c_{tR}} = \frac{\Delta_{tR}}{m_{\tilde{T}^c}}, \quad \frac{s_{bR}}{c_{bR}} = \frac{\Delta_{bR}}{m_{\tilde{B}^c}}, \quad M_{\tilde{T}} = \frac{M_{\tilde{T}^c}}{c_{tR}}, \quad M_{\tilde{B}} = \frac{M_{\tilde{B}^c}}{c_{bR}}. \tag{9}$$

The fact that the SM left-handed doublet mixes with two different sectors through Δ_{L1} and Δ_{L2} complicates the expressions for the corresponding rotations. They can be found in the $\Delta_{L2} \ll \Delta_{L1}$ limit in [20] and are reproduced, for further discussion, in Appendix A for the charge $-1/3$ sector. This limit is well motivated by the stringent constraints on the $Zb_L\bar{b}_L$ coupling (which receives corrections that are suppressed by the ratio Δ_{L2}/Δ_{L1}), it explains the fact that $m_b \ll m_t$ and it is naturally generated by the renormalization flow in the conformal phase [36]. In any case we will not make use of the explicit expressions since in practice we will use the top and bottom quark masses to (numerically) fix the values of Δ_{L1} and Δ_{L2} in terms of the remaining parameters of the model. We have checked that, in all the cases we have considered, the hierarchy $\Delta_{L2}/\Delta_{L1} \ll 1$ is preserved.

As we said, the top and bottom quark masses are used to fix the values of Δ_{L1} and Δ_{L2} . A third parameter, that we take θ_s can be fixed from the value of the strong coupling constant

$$\sin \theta_s = \frac{g_s}{g_c}. \quad (10)$$

All the other parameters, namely $g_c, Y_T, Y_B, M_{G^c}, M_Q, M_{Q'}, M_{\tilde{T}^c}, M_{\tilde{B}^c}, s_{tR}, s_{bR}$, can be allowed to vary. In order to reduce the dimensionality of the parameter space we have fixed all the composite fermion masses ¹ to a common one

$$M_Q = M_{Q'} = M_{\tilde{T}^c} = M_{\tilde{B}^c} \equiv M_F. \quad (\text{Universal Masses}) \quad (11)$$

Similarly we have fixed

$$Y_T = Y_B = 3, \quad (12)$$

as they are expected to be numbers somewhat larger than one. For each value of s_{tR}, s_{bR} and M_F the fermion spectrum is then completely fixed. Under the assumption of universal composite fermion masses, Eq. (11), the lightest new fermion is almost

¹ Note that these are the masses of the composite states before EWSB and before their mixing with the elementary states.

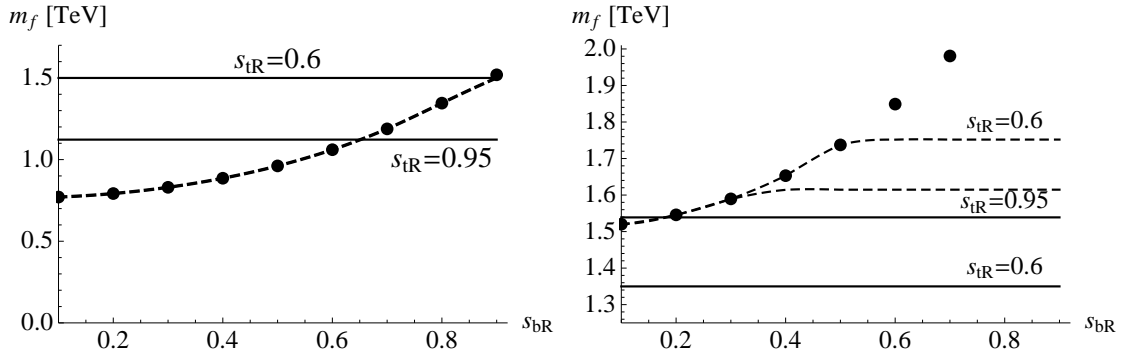


FIG. 1: Mass of the lightest charge $2/3$ (solid) and $-1/3$ (dashed) quark as a function of s_{bR} and for different values of s_{tR} . The dots correspond to the mass of B_H (see text). In the left panel we have used Eq. (11) with $M_F = 1.5$ TeV and in the right one we have used Eq. (13) with $M_Q = 1.5$ TeV.

always a charge $-1/3$ quark that decays, with 100% branching ratio, into Hb .² We show in the left panel of Fig. 1 the mass of the lightest charge $2/3$ (solid horizontal lines) and charge $-1/3$ (dashed line) new quarks as a function of s_{bR} and for two different values of s_{tR} , corresponding to a mildly ($s_{tR} = 0.6$) and very strongly ($s_{tR} = 0.95$) composite t_R , respectively. We have assumed $M_F = 1.5$ TeV (which corresponds to the mass of the charge $5/3$ and charge $-4/3$ new quarks). The dots in the figure represent the mass of the charge $-1/3$ new quark that decays predominantly (with 100% branching ratio for the parameters in the plot) into Hb . For a universal fermion mass this always agrees with the lightest one. Naturalness arguments and the observed value of the Higgs boson mass typically predict the lightest fermionic resonances to be the $(T_{5/3}^c, T_{2/3}^c)$ multiplet [5–9]. In order to test this scenario we have considered an alternative fermion mass configuration in which all multiplets are 50% heavier than Q ,

$$M_{Q'} = M_{\tilde{T}^c} = M_{\tilde{B}^c} = 1.5M_Q. \quad (\text{Lightest } Q). \quad (13)$$

² The 100% branching fraction into Hb has to do with the degenerate bidoublet structure of the model, see Appendix A. If the heavy particle involved was an electroweak doublet, instead of a custodial bidoublet, we would get $BR(B_H \rightarrow Hb) = BR(B_H \rightarrow Zb) = 50\%$.

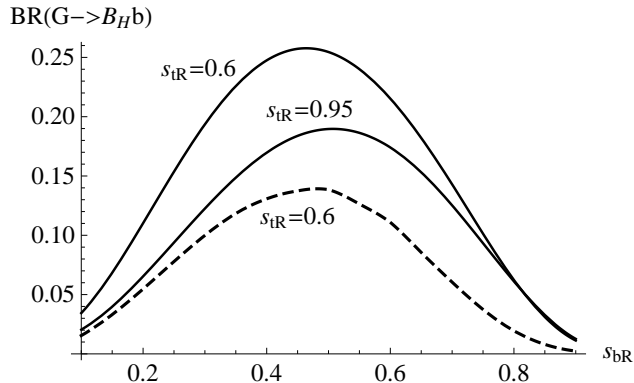


FIG. 2: Branching ratio of the heavy gluon into $B_H\bar{b} + \bar{B}_H b$ as a function of s_{bR} and for different values of s_{tR} . We use solid lines for the choice of fermion masses in Eq. (11) and dashed lines for Eq. (13). We have fixed $M_{G^*} = 2.5$ TeV, $g_c = 3$ and the mass of the fermion resonances are fixed so that the lightest new fermion has a mass $M_{G^*}/2$.

The resulting spectrum of lightest modes, for $M_Q = 1.5$ TeV is shown in the right panel of Fig. 1 with the same notation than in the left panel of the figure. The masses of the charge $5/3$ and $-4/3$ quarks are in this case 1.5 TeV and 2.25 TeV, respectively. The mass of the lightest charge $-1/3$ quark now depends on the degree of compositeness of t_R and the one decaying predominantly into Hb is not always the lightest one. Still there is a relatively light charge $-1/3$ quark with a 100% branching ratio into Hb . In the following we will denote this quark, which is the one we will be focusing on in this work, B_H .

Once we have discussed the features of the fermionic spectrum and their decay patterns, we turn our attention to the only two remaining parameters in the model, namely the heavy gluon, M_{G^*} , mass and the composite coupling, g_c . In order to avoid too large a width for the heavy gluon we will choose its mass so that pair production of top and bottom partners is kinematically forbidden. Thus, we fix the mass of the heavy gluon to have twice the mass of the lightest new fermion after EWSB. In practice what we do is to choose a value for M_{G^*} and fix the value of M_F that makes the mass of the lightest new fermion $M_{G^*}/2$. Once the value of M_{G^*} is

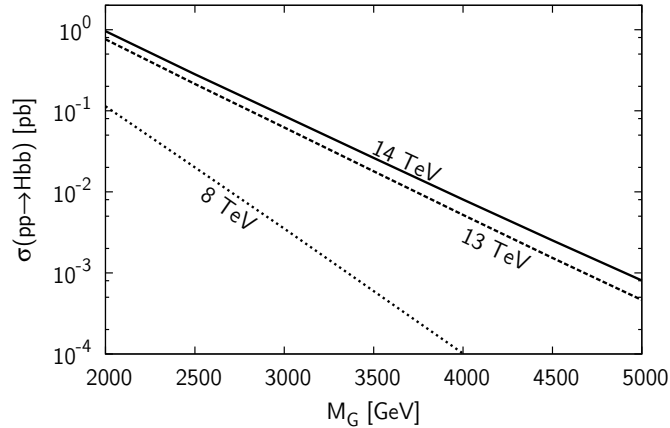


FIG. 3: $Hb\bar{b}$ production cross section in the benchmark model, Eqs. (11,12), with $g_c = 3$, as a function of M_{G^*} . M_F in Eq. (11) has been chosen such that the lightest fermionic resonance has a mass $M_{G^*}/2$.

fixed, all the phenomenological implications of the model can be worked out. We show in Fig. 2 the branching ratio of the heavy gluon into $B_H\bar{b} + \bar{B}_H b$ as a function of s_{bR} for different values of s_{tR} . Solid and dashed lines are used for benchmarks Eq. (11) and Eq. (13), respectively. We have fixed $M_{G^*} = 2.5$ TeV and $g_c = 3$ in this figure. The bell-like shape of the figure arises from the fact that the coupling between the heavy gluon and $b_R B_{HR}$ is proportional to $s_{bR} c_{bR}$ (see Appendix A).

III. $Hb\bar{b}$ VIA SINGLE PRODUCTION OF TOP/BOTTOM PARTNERS

As we have discussed in the previous section, the heavy gluon can have a sizeable decay branching ratio into $B_H\bar{b} + \bar{B}_H b$, where B_H is a charge $-1/3$ quark that is typically relatively light and decays always to Hb . Thus, single production of B_H via the s-channel exchange of G^* results in an $Hb\bar{b}$ final state with a significant production cross section. We show in Fig. 3 the $Hb\bar{b}$ production cross section, as a function of the heavy gluon mass, with the parameters fixed according to Eqs. (11) and (12), $g_c = 3$ and M_F chosen such that the lightest new fermion has a

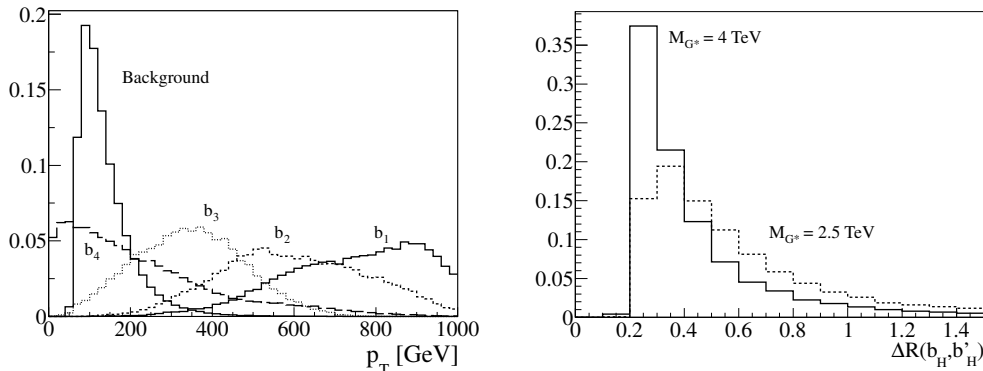


FIG. 4: Left: Parton level p_T distribution of the 4 b quarks in the signal (denoted in decreasing order of p_T by $b_{1,2,3,4}$) and of the hardest b quark in the irreducible $4b$ background. Right: ΔR separation between the two b -quarks from the Higgs decay at the partonic level for two different values of the heavy gluon mass. The mass of the heavy bottom is in both cases $M_{B_H} = M_{G^*}/2$. All distributions are normalized to unit area.

mass equal to $M_{G^*}/2$. This production cross section is sizeable but not large enough to allow us to use the cleaner $H \rightarrow \gamma\gamma, ZZ^*$ decay channels. Among the two leading decay channels, we have found that the $H \rightarrow b\bar{b}$ is the most promising one. The main reasons are the large number of b quarks in the final state, which is a very powerful discriminator against the background, together with very special kinematics inherited from the large masses of G^* and B_H . As we now show, the latter ensures a clean trigger and a very simple reconstruction algorithm.

The process we are interested in is therefore

$$pp \rightarrow G^* \rightarrow B_H \bar{b} + \bar{B}_H b \rightarrow H b \bar{b} \rightarrow 4b. \quad (14)$$

Due to the large masses we can probe at the LHC, all four b quarks in the final state are very hard. We show in Fig. 4 (left) the p_T distribution of the four b quarks at the partonic level, for a heavy gluon mass $M_{G^*} = 2.5$ TeV, together with the p_T distribution of the hardest b quark for the irreducible $4b$ QCD background (distributions are normalized to unit area). All four b -jets are quite hard with the p_T of the two leading jets well above 300 and 200 GeV, respectively. This allows for a

very clean trigger of the signal events and also for the possibility of hard cuts on the p_T of the leading b -jets, an important ingredient to bring the irreducible background down to manageable levels.

One important feature is that, due to the relatively large mass of B_H , the Higgs boson tends to be quite boosted and its decay products relatively aligned. We show in Fig. 4 (right) the ΔR separation between the two b -quarks that reconstruct the Higgs, at the partonic level, for two different values of M_{G^*} (recall that we have $M_{B_H} = M_{G^*}/2$). We find that less than 35% of the events have $\Delta R < 0.4$ for $M_{G^*} = 2.5$ TeV. This number goes up to 60% for $M_{G^*} = 4$ TeV. Thus, it is clear that for larger heavy gluon masses, the use of boosted techniques [39, 40] is likely to enhance the sensitivity. However, we have decided to restrict ourselves to traditional techniques because the use of one less b -tag would force us to consider new background processes that are difficult to estimate with other means than data-driven methods.

IV. EXPERIMENTAL ANALYSIS

In this section we describe a very simple experimental analysis that takes advantage of the kinematical features discussed in the previous section to disentangle the signal from the background. In our simulations we have used **MadGraph v4** [41] and **AlpGen v2.13** [42] for parton level signal and background generation, respectively. We have set the factorization and renormalization scales to the default values and used the CTEQ6L1 PDFs [43]. We have used **Pythia v6** [44] for parton showering and hadronization and **Delphes v1.9** [45] for fast detector simulation. Jets are reconstructed using the anti-kt algorithm with $R = 0.4$, and we are assuming a value of 0.7 for the b -tagging efficiency. Jets and charged leptons used in our analysis are defined to have $p_T^j > 20$ GeV. Charged leptons are also required to be well isolated from jets with $\Delta R(lj) > 0.4$. We have considered two different configurations for the LHC parameters with benchmark values $\sqrt{s} = 8$ TeV and an integrated lumi-

luminosity of 20 fb^{-1} (LHC8) and $\sqrt{s} = 14 \text{ TeV}$ with an integrated luminosity of 100 fb^{-1} (LHC14).

The main background to the $pp \rightarrow G^* \rightarrow B_H \bar{b} + \bar{B}_H b \rightarrow H b \bar{b} \rightarrow 4b$ process we are interested in comes from the irreducible QCD $4b$ production. Other purely hadronic backgrounds are suppressed by the small b-tagging fake-rate (we conservatively set $1/100$ for light jets and $1/10$ for c-jets) and can be neglected. The same happens to other SM processes in which at least one isolated lepton is produced (we will impose a lepton veto to reduce these to negligible levels). Thus, the only background we have to consider is the irreducible one. Still, the QCD $4b$ cross section is so large that we have been forced to generate events in the phase space region defined by $p_T^b > 50 \text{ GeV}$ and $\Delta R(b, b) > 0.3$ to have a large enough sample. The cross section in this region of parameter space is $\sim 12 \text{ pb}$. In order to ensure enough statistics we have generated a number of events corresponding to a luminosity of $\sim 1 \text{ ab}^{-1}$. In light of the results of NLO studies [46, 47] we have assumed that the shape in the p_T distributions is well described by our leading order calculations but the total cross section must be corrected with a k-factor that we conservatively set to 1.5.

In order to bring the irreducible background down to manageable levels, we impose the following set of cuts:

$$\begin{aligned}
 N_b \geq 4, \quad N_l = 0, \quad p_T(b) \geq & \begin{cases} 50 \text{ GeV (LHC8)}, \\ 60 \text{ GeV (LHC14)}, \end{cases} \\
 p_T(b_1) \geq & \begin{cases} 200 \text{ GeV (LHC8)}, \\ 300 \text{ GeV (LHC14)}, \end{cases} \quad p_T(b_2) \geq & \begin{cases} 100 \text{ GeV (LHC8)}, \\ 200 \text{ GeV (LHC14)}, \end{cases} \\
 |m_{b_H b'_H} - m_H| \leq & 30 \text{ GeV}, \tag{15}
 \end{aligned}$$

where we have denoted $b_{1,2,\dots}$ the b -jets in decreasing order in p_T , b generically denotes all b -jets and finally b_H and b'_H are the two b -jets that better reconstruct the Higgs. We impose different cuts on the p_T of the b -jets for LHC8 and LHC14. We now use the invariant mass of the four leading b -jets as the discriminating variable. We require the events to have a $4b$ invariant mass close to the test mass for the heavy

8 TeV	N_b	N_l	p_T^b	$p_T^{b_1}$	$p_T^{b_2}$	$ m_{bb} - m_H $	$m(4b)$
Signal	16	99	68	99	99	56	89
Background	17	99	10	13	89	46	0.7
14 TeV							
Signal	16	99	59	98	98	59	92
Background	20	99	12	7.6	63	36	11

TABLE I: Cut by cut efficiencies (in percent) for the signal in the benchmark model with $M_{G^*} = 2.5$ TeV for two different center of mass energies, and the irreducible $b\bar{b}b\bar{b}$ background. The slightly low efficiency in N_b for the signal is consequence of the boosted regime.

gluon:

$$M_{G^*} + 1000 \text{ GeV} < m_{4b} < M_{G^*} + 500 \text{ GeV}. \quad (16)$$

The efficiencies of the different cuts for the signal (with $M_{G^*} = 2.5$ TeV) and the irreducible background are given in Table I. The relatively low efficiency for the signal of the N_b cut is due to the fraction of boosted events. We show in Fig. 5 (left) the invariant mass of the four leading b -jets, after the cuts in Eq. (15) have been imposed, for the signal and irreducible background. The figure shows that this observable is clearly a discriminating variable, with a distinct peak around the mass of the heavy gluon. Cutting on a window around the test mass, the background is reduced to negligible levels. Once we have reconstructed the heavy gluon mass, we can reconstruct the heavy bottom by taking the invariant mass of the two b -tagged jets that best reconstruct the Higgs mass (b_H and b'_H) and the leading one among the remaining b -jets (denoted b_{lead}). We have checked that the peak in this distribution around the heavy bottom mass is narrower than the one obtained with other combinations of b -jets, for the values of M_{B_H} and M_{G^*} we have considered. An example of this is shown in the right panel of Fig. 5.

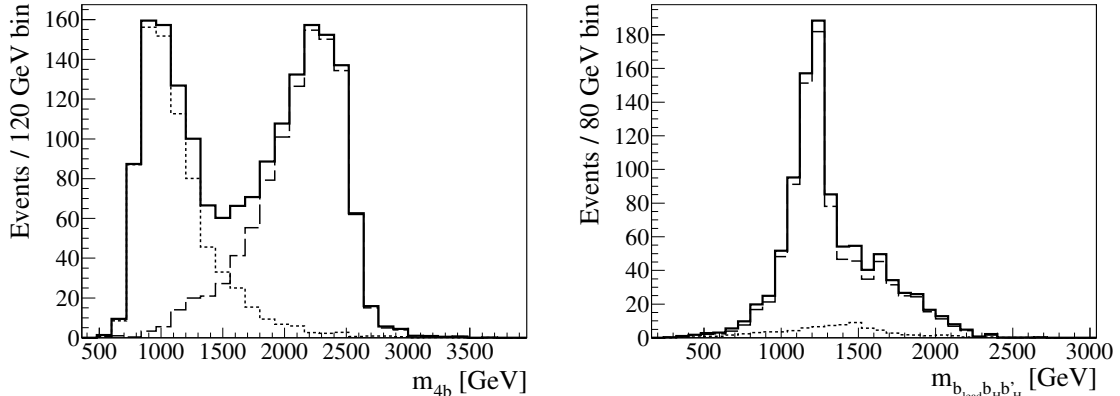


FIG. 5: Plots of reconstructed events after the cuts of equation (15). The dashed, dotted and solid lines represent the signal, the background and the sum (data) respectively. Left) reconstruction of G^* from the four leading b -tagged jets. Right) reconstruction of B_H from the two jets reconstructing the Higgs plus the hardest among the remaining b -jets after the cuts in Eqs. (15) and (16).

V. DISCUSSION OF THE RESULTS

The analysis described in the previous section takes full advantage of the kinematical features of the signal to extract it from the background. Other searches, not specifically aimed at this model can be somewhat sensitive to the signal we are considering. Among them, the two most important ones are searches with many b -quarks in the final state, typically motivated by supersymmetric models, and searches for new physics in dijet final states. The latter has been shown to impose stringent constraints on these kind of models [21] but they are less related to the particular final state that we are considering in this work. We have found that, among the former, searches for $Hb\bar{b}$ production in supersymmetric models and searches for multi- b final states in association with missing energy are the most sensitive ones. Let us discuss them in turn.

Searches for $Hb\bar{b}$ (or Hb) in supersymmetry look for events with three or more relatively hard b -jets in the final state and try to reconstruct the Higgs from the two

leading b -jets. The expected p_T distribution of the signal in supersymmetric models is much softer than in our model and therefore the focus is in a highly background populated region in which our signal gets easily diluted. This fact, combined with the small luminosity, makes these searches not very sensitive to our model, although a very simple extension of the analysis with harder cuts on the p_T of the b -tagged jets would make them a very sensitive probe of composite Higgs models.

Searches for multi- b final states in association with missing energy, on the other hand, look for signatures with many b -jets in the final state, with a large value of H_T (scalar sum of all the b -jet p_T) and a sizeable amount of missing transverse energy. Due to the large energy of the final state particles in our model, the fake missing transverse energy is non-negligible and these searches are sensitive to our model. It is interesting to note that analyses in which sophisticated observables are used to avoid contamination from fake missing E_T (like α_T in [48]) kill our signal together with the multi-jet background. However, other analyses in which the rejection of fake missing energy is less sophisticated impose some constraints on the parameter space of our model. We have used [49] that analyzes the full 8 TeV LHC data and show that, although this search imposes some constraints on the model, our modified analysis in which the missing energy requirement is replaced for a more stringent requirement in terms of the p_T of the different b -jets, leads to a much better reach. This is an example of a very simple modification of current analyses that could maximize the number of models the searches are sensitive to.

Once we have described the experimental analysis and our results for the corresponding efficiencies we can report on the expected bounds and discovery reach at the LHC. Our main result, summarized in Fig. 6, shows the expected 95% C.L. upper limit on the $Hb\bar{b}$ production cross section as a function of the heavy gluon mass. We overlay the cross sections for several points in parameter space for our model that allow us to compute the corresponding bounds on M_{G^*} . The results for the LHC8 are shown in the left panel of the figure in which we also show the corresponding bound from current searches on multi- b plus missing energy final states.

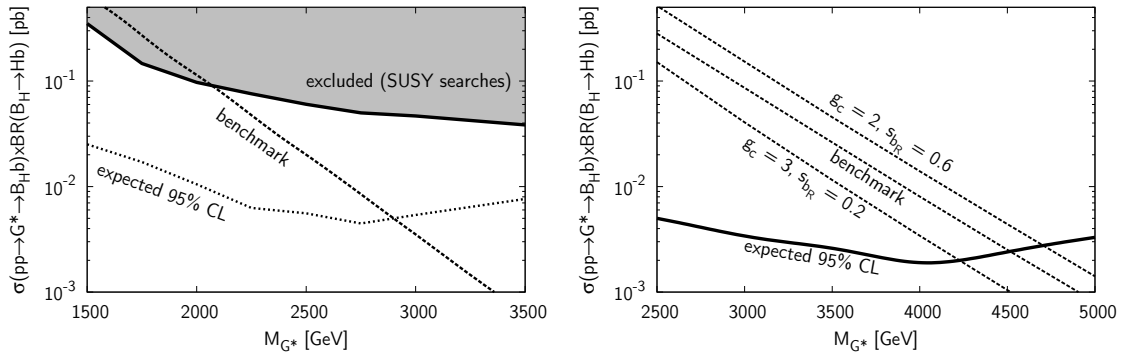


FIG. 6: 95% C.L. exclusion bound on the $Hb\bar{b}$ production cross section as a function of the heavy gluon mass for the LHC8 (left) and LHC14 (right) with 20 fb^{-1} and 100 fb^{-1} of integrated luminosity, respectively. The dashed lines correspond to the cross section in our model for different values of the input parameters.

As we see, our modified analysis can improve the current limits (using the same data) by more than an order of magnitude in cross section and by almost 1 TeV in the reach of the heavy gluon mass up to $\sim 3 \text{ TeV}$ for the benchmark model. The expected bound for the LHC14, together with several different models is shown in the right panel of the figure. In this case 100 fb^{-1} of integrated luminosity would allow us to probe masses in the $4 - 5 \text{ TeV}$ region for the heavy gluon, depending on the model parameters.

The sensitivity of the LHC8 and LHC14 to different parameters in the model is shown in Fig. 7 in which we give the sensitivity that can be reached, as a function of s_{bR} (left) and g_c (right), for different values of the heavy gluon mass and for the two LHC configurations with LHC8 on the top row and LHC14 on the bottom one. In order to account for the finite statistics, we use `SigCalc` [50], that takes $\tau \equiv \mathcal{L}_{\text{MC}}/\mathcal{L}_{\text{data}}$ as an input, where $\mathcal{L}_{\text{data}}$ and \mathcal{L}_{MC} represent the actual and the generated luminosities respectively. The results given by `SigCalc` reduces to

$$\mathcal{S}(s, b) = \sqrt{2 \left((s + b) \log \left(1 + \frac{s}{b} \right) - s \right)} \quad (17)$$

in the limit $\tau \rightarrow \infty$. In this plot we also show the bounds derived from dijet

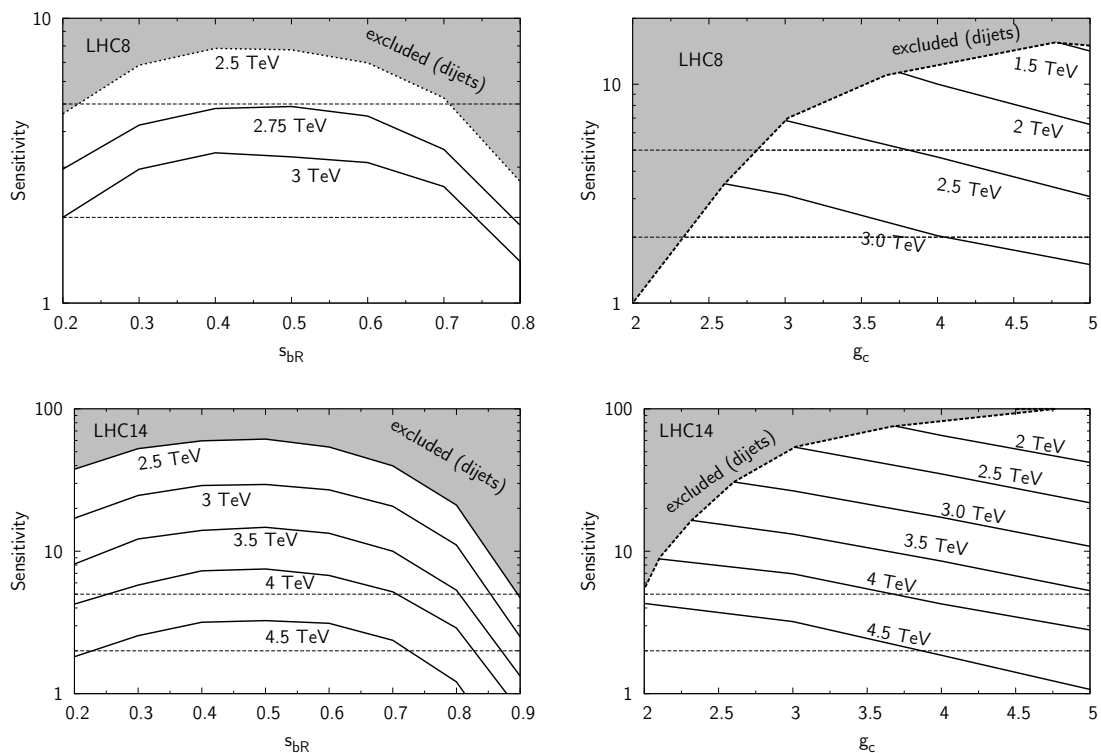


FIG. 7: Sensitivity reach in the model as a function of s_{bR} (left) and g_c (right), for the LHC8 with 20 fb^{-1} (top) and the LHC14 with 100 fb^{-1} (bottom). The bounds from current dijet searches are also shown.

searches [51], which are more constraining than multi- b searches for our model. As we see, despite the stringent bounds on the model from dijet searches, there are allowed regions in parameter space with heavy gluon masses in the $1.5 - 2.75 \text{ TeV}$ range that could be discovered with the LHC8 data. At the LHC14 masses up to 5 TeV can be constrained and up to 4.5 TeV discovered with 100 fb^{-1} .

VI. CONCLUSIONS

Light top and bottom partners are a common prediction of natural models of strong electroweak symmetry breaking. They are new vector-like quarks that play a direct role in the way the top and bottom quarks acquire their mass (and their

partners under the global symmetries of the composite sector). Among these top and bottom partners, we can have a charge $-1/3$ new quark, heavy bottom, that decays predominantly into Hb . The single production of this heavy bottom via the s-channel exchange of a heavy gluon, a color octet vector resonance that is also a common prediction in these models, results in a sizeable $Hb\bar{b}$ production. Contrary to what happens in supersymmetric models, this large $Hb\bar{b}$ production cross section is not related to an enhancement of the bottom quark Yukawa coupling but to the strong couplings among resonances of the composite sector. Also, in our case, the relatively large masses of the intermediate states ensures that we can use the leading $H \rightarrow b\bar{b}$ Higgs decay, as all the particles in the final state are quite hard. This guarantees a clean trigger and a powerful discriminating power against the large QCD background.

We have shown that simple modifications of current multi- b final state searches, typically motivated by supersymmetric models, can turn these analyses into very powerful probes of composite Higgs models. The requirement of very stringent cuts on the p_T of the different b -tagged jets and a relaxation in the amount of missing energy requested can significantly reduce the background without sensibly affecting our signal. In this way, masses up to ~ 3 (2.75) TeV for the heavy gluon can be excluded (discovered) with current data at the LHC8. The bounds and discovery limits go up to ~ 5 and 4.5 TeV, respectively at the LHC14 with 100 fb^{-1} of integrated luminosity.

We have also shown that electroweak symmetry breaking effects can substantially modify the collider phenomenology of bottom partners. The small coupling between the latter and the bottom quark, together with the very large coupling among composite states can lead to a puzzling situation from the experimental point of view in which heavy states, well above the LHC reach, have a profound impact on the phenomenology of new discovered particles. This effect is explained in detail in Appendix A and shows that simplified models can be a good first approach to new physics searches but they can also miss some of the main phenomenological proper-

ties of realistic models of new physics. This is particularly true on models of strong EWSB, in which large couplings among heavy states are naturally expected.

Acknowledgments

We would like to thank F. del Águila, G. Azuelos and N. F. Castro for useful comments. This work has been supported by MICINN projects FPA2006-05294 and FPA2010-17915, through the FPU programme and by Junta de Andalucía projects FQM 101, FQM 03048 and FQM 6552.

Appendix A: Slow decoupling of heavy partners in models of strong electroweak symmetry breaking

In this appendix we will explain why the lightest charge $-1/3$ new quark decays predominantly in the Hb channel. We will also show that the features of models of strong EWSB with partial compositeness can lead to the following situation: a single new quark, with electric charge $-1/3$, is found at the LHC but its decay pattern differs substantially from the one expected for a vector-like singlet quark. This is most easily understood in the basis in which we have diagonalized the mass matrix before EWSB. As we mentioned in the text, the presence of Δ_{L1} and Δ_{L2} makes this diagonalization non-trivial. Approximate analytic expressions can be obtained in the limit $\Delta_{L2} \ll M$, with M any of the dimensionful parameters in the Lagrangian of Eq. (5). This limit is well motivated by the fact that corrections to the $Zb_L\bar{b}_L$ coupling scale like Δ_{L2}^2 and experimental bounds on this coupling therefore imply that $\Delta_{L2} \ll M$. Furthermore, the bottom quark mass is also proportional to Δ_{L2} and we can relate the absence of large corrections to the $Zb_L\bar{b}_L$ coupling with the fact that $m_b \ll m_t$. Finally, the choice $\Delta_{L2} \ll \Delta_{L1}$ is radiatively stable.

The mass matrix for charge $-1/3$ quarks in the $b, \tilde{B}, B', B_{-1/3}, B$ basis reads [52]

$$\mathcal{M}_{-1/3} = \begin{pmatrix} \frac{v}{\sqrt{2}}Y_B s_2 s_{bR} & -\frac{v}{\sqrt{2}}Y_B s_2 c_{bR} & 0 & 0 & 0 \\ 0 & \frac{M_{\tilde{B}^c}}{c_{bR}} & \frac{v}{\sqrt{2}}Y_B & \frac{v}{\sqrt{2}}Y_B & \frac{v}{\sqrt{2}}Y_B s_4 \\ -\frac{v}{\sqrt{2}}Y_B s_{bR} & \frac{v}{\sqrt{2}}Y_B c_{bR} & M_{Q'} & 0 & 0 \\ -\frac{v}{\sqrt{2}}Y_B s_{bR} & \frac{v}{\sqrt{2}}Y_B c_{bR} & 0 & M_{Q'} & 0 \\ -\frac{v}{\sqrt{2}}Y_B s_{bR} s_3 & \frac{v}{\sqrt{2}}Y_B c_{bR} s_3 & 0 & 0 & \sqrt{M_Q^2 + \Delta_{L1}^2} \end{pmatrix} + \mathcal{O}(\Delta_{L2}^2/M^2), \quad (\text{A1})$$

where

$$s_2 \equiv \Delta_{L2} \frac{M_Q}{M_{Q'} \sqrt{\Delta_{L1}^2 + M_Q^2}}, \quad (\text{A2})$$

$$s_3 \equiv \Delta_{L2} \frac{\Delta_{L1} M_{Q'}}{(\Delta_{L1}^2 + M_Q^2 - M_{Q'}^2) \sqrt{\Delta_{L1}^2 + M_Q^2}}, \quad (\text{A3})$$

$$s_4 \equiv \Delta_{L2} \frac{\Delta_{L1}}{\Delta_{L1}^2 + M_Q^2 - M_{Q'}^2}. \quad (\text{A4})$$

Note that $s_{2,3,4}$ are all proportional to Δ_{L2} and are therefore expected to be small. The fields of this basis are written in terms of the elementary and composite states as follows:

$$b_L = c_1 b_L^c - s_1 B_L^c - s_2 B_L'^c, \quad b_R = c_{bR} b_R^e - s_{bR} \tilde{B}_R^c, \quad (\text{A5})$$

$$B_L = s_1 b_L^c + c_1 B_L^c + s_3 B_L'^c, \quad B_R = B_R^c + s_4 B_R'^c, \quad (\text{A6})$$

$$B_L' = (s_2 c_1 - s_1 s_3) b_L^c - (c_1 s_3 + s_1 s_2) B_L^c + B_L'^c, \quad B_R' = B_R'^c - s_4 B_R^c, \quad (\text{A7})$$

$$B_{-1/3L} = B_{-1/3L}^c, \quad B_{-1/3R} = B_{-1/3R}^c, \quad (\text{A8})$$

$$\tilde{B}_L = \tilde{B}_L^c, \quad \tilde{B}_R = s_{bR} b_R^e + c_{bR} \tilde{B}_R^c, \quad (\text{A9})$$

where

$$s_1 = \frac{\Delta_{L1}}{\sqrt{\Delta_{L1}^2 + M_Q^2}}, \quad (\text{A10})$$

and $c_i = \sqrt{1 - s_i^2}$ for $i = 1, \dots, 4$. In this basis, the heavy gluon has the following off-diagonal couplings

$$\mathcal{L} = \frac{g_s}{\sin \theta_s \cos \theta_s} G_\mu^* \left[s_1 c_1 \bar{b}_L \gamma^\mu B_L + s_{bR} c_{bR} \bar{b}_R \gamma^\mu \tilde{B}_R + \text{h.c.} \right] + \dots, \quad (\text{A11})$$

where we have neglected terms that are suppressed by Δ_{L2}/M . The mass matrix in Eq. (A1) can be further simplified by means of the following rotation

$$B_{L,R}^{\pm} = \frac{\pm B'_{L,R} + B_{-1/3 L,R}}{\sqrt{2}}. \quad (\text{A12})$$

In the new basis $b, \tilde{B}, B^+, B^-, B$, the mass matrix reads

$$\mathcal{M}'_{-\frac{1}{3}} = \begin{pmatrix} \frac{v}{\sqrt{2}} Y_B s_2 s_{bR} & -\frac{v}{\sqrt{2}} Y_B s_2 c_{bR} & 0 & 0 & 0 \\ 0 & \frac{M_{\tilde{B}c}}{c_{bR}} & v Y_B & 0 & \frac{v}{\sqrt{2}} Y_B s_4 \\ -v Y_B s_{bR} & v Y_B c_{bR} & M_{Q'} & 0 & 0 \\ 0 & 0 & 0 & M_{Q'} & 0 \\ -\frac{v}{\sqrt{2}} Y_B s_{bR} s_3 & \frac{v}{\sqrt{2}} Y_B c_{bR} s_3 & 0 & 0 & \sqrt{M_Q^2 + \Delta_{L1}^2} \end{pmatrix}. \quad (\text{A13})$$

Recall that $s_{2,3,4}$ are expected to be small. In this case, all the Yukawa couplings inducing mixing among the different quarks are suppressed except for the ones between \tilde{B} and B^+ , which are large (recall that we expect $Y_B \sim \mathcal{O}(\text{a few})$), and the coupling of B_L^+ and b_R will again be unsuppressed except for very small values of s_{bR} . Under the assumption of universal masses, $M_{\tilde{B}c} = M_Q = M_{Q'}$, the lightest charge $-1/3$ quark is then a combination of \tilde{B} and B^+ that inherits the sizeable coupling to the heavy gluon from its \tilde{B} component and the overwhelming decay into Hb from its B^+ component.³

The large coupling between B^+ and \tilde{B} , together with the suppressed coupling between \tilde{B} and the SM bottom quark can lead to an interesting situation in which the heavy partners show a very slow decoupling. In order to see this effect, let us consider the limit in which the only light new quark is \tilde{B}

$$v \ll M_{\tilde{B}c} \ll M_Q \sim M_{Q'}, \quad (\text{slow decoupling}). \quad (\text{A14})$$

In particular we consider that \tilde{B} is well within the LHC reach whereas all other particles are well above the LHC threshold. The small value of s_3 and s_4 allow us

³ B^{\pm} are the symmetric and antisymmetric combinations of quarks with third component of isospin $T_L^3 = \pm 1/2$, respectively. In the absence of any further mixing they have the following decay pattern $BR(B^+ \rightarrow Hb) = BR(B^- \rightarrow Zb) = 1$. See [53–56] for a detailed discussion and collider implications.

to disregard the B^- and B fields in the following and focus the discussion in b, \tilde{B} and B^+ . In the limit in which $M_{Q'} \rightarrow \infty$, \tilde{B} is an electroweak singlet and will have the standard decay pattern

$$BR(\tilde{B} \rightarrow Wt)/BR(\tilde{B} \rightarrow Zb)/BR(\tilde{B} \rightarrow Hb) \approx 2/1/1. \quad (\text{A15})$$

The large coupling between \tilde{B} and B^+ forces a sizeable mixing between the two and the lightest mode then inherits part of the peculiar (because of the large branching ratio) decay mode of B^+ into Hb . This effect is suppressed by powers of $M_{Q'}$ but the large value of the couplings and the fact that it is competing with the suppressed coupling of \tilde{B} with b , means that very large values of $M_{Q'}$ are required before the decoupling is effective. In order to be more specific, let us focus on the physical Yukawa couplings (after EWSB) between the bottom quark and the lightest new quark of charge $-1/3$, that we will call B_l . The relevant part of the Lagrangian reads

$$\mathcal{L} = \frac{H}{\sqrt{2}} \bar{b} [\lambda_{bB_l} P_R + \lambda_{B_l b} P_L] B_l + \text{h.c.} + \dots, \quad (\text{A16})$$

where $P_{L,R} = (1 \mp \gamma^5)/2$ are the standard chirality projectors. In the slow decoupling limit of Eq.(A14) we can obtain approximate analytic expressions for these couplings

$$\begin{aligned} \lambda_{bB_l} = & -Y_B s_2 c_{bR} + \frac{1}{2} Y_B^3 s_2 c_{bR} (1 - 3s_{bR}^2) \left(\frac{s_2^2 v^2}{2 M_{\tilde{B}}^2} - \frac{v^2}{M_{Q'}^2} \right) \\ & - Y_B^3 s_2 (2 - 3s_{bR}^2) \frac{v^2}{M_{\tilde{B}} M_{Q'}} + \mathcal{O} \left(\frac{v^4}{M^4}, \frac{v^2 M_{\tilde{B}}}{M_{Q'}^3} \right), \end{aligned} \quad (\text{A17})$$

$$\lambda_{B_l b} = -Y_B^2 s_2^2 s_{bR} c_{bR} \frac{v}{\sqrt{2} M_{\tilde{B}}} + 2\sqrt{2} Y_B^2 s_{bR} \frac{v}{M_{Q'}} + \mathcal{O} \left(\frac{v^3}{M^3}, \frac{v M_{\tilde{B}}}{M_{Q'}^2} \right). \quad (\text{A18})$$

The first term in Eq. (A17) is the one that would determine the decay pattern of B_l if it came mainly from a vector-like singlet, resulting in the well known 2 : 1 : 1 pattern, see Eq. (A15). This coupling receives corrections from the presence of B^+ , like the one in the second line of Eq. (A17) that can easily exceed the otherwise leading term. Even more important in our example is the fact that the $\lambda_{B_l b}$, which is irrelevant in the case of a vector-like singlet, receives huge corrections that can

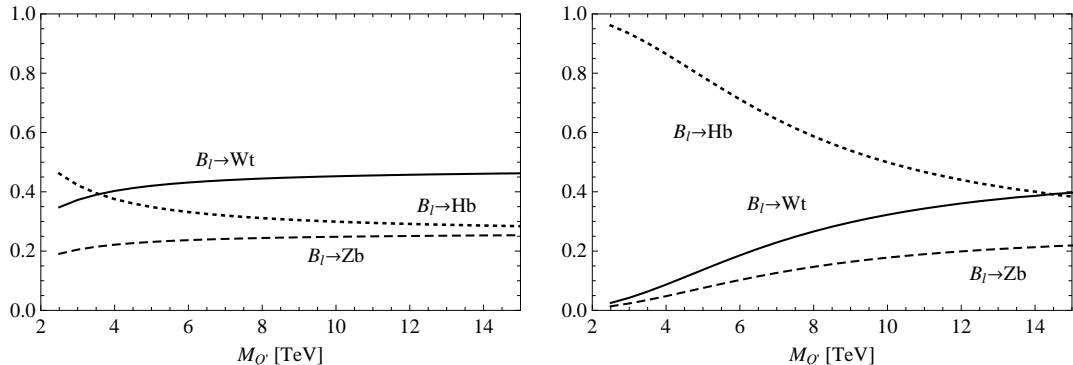


FIG. 8: Branching fraction decay of B_l as a function of $M_{Q'}$ for $s_{bR} = 0.05$ (left) and $s_{bR} = 0.2$ (right). We have fixed $M_{B_l} = 1$ TeV and $M_Q = M_{Q'}$.

dramatically change the decay pattern of B_l . Explicitly, for the leading correction, which corresponds to the second term in Eq. (A18) to be much smaller than the first term in λ_{bB_l} , so that the decay pattern becomes again the standard one, we need the mass of B^+ to be

$$M_{Q'} \gg \frac{2s_{bR}^2 Y_B^2 v^2}{c_{bR} m_b} \approx 272 \frac{s_{bR}^2}{c_{bR}} \left(\frac{Y_B}{3}\right)^2 \text{ TeV}, \quad (\text{A19})$$

where we have used that the bottom quark mass is approximately given by

$$m_b \approx Y_B s_2 s_{bR} \frac{v}{\sqrt{2}}. \quad (\text{A20})$$

This is a very conservative estimate of the mass scale at which B^+ stops having a profound impact on the decay pattern of B_l . A more quantitative result is given in Fig. 8 in which we show the branching ratios of B_l as a function of $M_{Q'}$ for $s_{bR} = 0.05$ (left) and $s_{bR} = 0.2$ (right). We have chosen the value of $M_{\bar{B}}$ so that the mass of the lightest new quark is $M_{B_l} = 1$ TeV. All the remaining masses are set equal to $M_{Q'}$. As we see, even for very small values of $s_{bR} \sim 0.05$ extra quarks with masses in the 3 – 5 TeV region still have an important impact on the decay pattern of B_l . This moves up to 15 TeV for $s_{bR} = 0.2$. In fact, for $s_{bR} \gtrsim 0.2$ we could have the challenging situation in which the only discovered new particle at the LHC is B_l but its decay patterns differ dramatically from the ones of a vector-like singlet. This is

due to its mixing with new quarks with masses $\sim 10 - 20$ TeV and would therefore escape experimental scrutiny even with an upgraded energy phase of the LHC.

Appendix B: Singlet scalar searches in Composite Higgs Models

Non-minimal composite Higgs models [29–34] can contain extra neutral singlets η in the spectrum of pseudo-Nambu-Goldstone bosons. This happens for instance in the case of the $SO(6)/SO(5)$ [29] or $SO(7)/G_2$ [33] cosets, in which the scalar Lagrangian has an $\eta \rightarrow -\eta$ symmetry that is only broken by couplings to the SM elementary fermions⁴. Thus, η can couple linearly to fermions but with a coupling suppressed by a factor $1/f$, with f the compositeness scale, through the operator

$$\mathcal{O} = \frac{cY}{f} \eta \bar{\psi}_L H \psi_R, \quad (\text{B1})$$

where Y is the fermion Yukawa coupling and c is expected to be order one (other dimension 5 operators are equivalent to this one via the classical equations of motion). The main standard production mechanism for η would then be gluon fusion but with a rate that is suppressed by a factor v^2/f^2 with respect to the SM Higgs gluon fusion production. In addition, the main decay of η is into a $b\bar{b}$ final state for masses below ~ 350 GeV, which suffers from a huge QCD background. Thus, in these cases, process similar to the one we have considered in this work, with the replacement of H with η ,

$$pp \rightarrow G^* \rightarrow B_\eta \bar{b} + \bar{B}_\eta b \rightarrow \eta b\bar{b} \rightarrow 4b, \quad (\text{B2})$$

could provide the leading channel to discover the composite singlets.

⁴ A vacuum expectation value for η could generate an ηHH coupling from the loop-induced scalar potential. In explicit models, however, a large region of parameter space is compatible with $\langle \eta \rangle = 0$ [6]

-
- [1] J. Santiago, PoS **ICHEP2010**, 557 (2010), 1103.4114.
- [2] K. Agashe, R. Contino, and A. Pomarol, Nucl.Phys. **B719**, 165 (2005), hep-ph/0412089.
- [3] K. Agashe and R. Contino, Nucl.Phys. **B742**, 59 (2006), hep-ph/0510164.
- [4] G. F. Giudice, C. Grojean, A. Pomarol, and R. Rattazzi, JHEP **0706**, 045 (2007), hep-ph/0703164.
- [5] O. Matsedonskyi, G. Panico, and A. Wulzer, JHEP **1301**, 164 (2013), 1204.6333.
- [6] M. Redi and A. Tesi, JHEP **1210**, 166 (2012), 1205.0232.
- [7] D. Marzocca, M. Serone, and J. Shu, JHEP **1208**, 013 (2012), 1205.0770.
- [8] A. Pomarol and F. Riva, JHEP **1208**, 135 (2012), 1205.6434.
- [9] G. Panico, M. Redi, A. Tesi, and A. Wulzer, JHEP **1303**, 051 (2013), 1210.7114.
- [10] M. S. Carena, E. Ponton, J. Santiago, and C. E. M. Wagner, Nucl.Phys. **B759**, 202 (2006), hep-ph/0607106.
- [11] M. S. Carena, E. Ponton, J. Santiago, and C. Wagner, Phys.Rev. **D76**, 035006 (2007), hep-ph/0701055.
- [12] C. Anastasiou, E. Furlan, and J. Santiago, Phys.Rev. **D79**, 075003 (2009), 0901.2117.
- [13] M. Carena, A. D. Medina, B. Panes, N. R. Shah, and C. E. Wagner, Phys.Rev. **D77**, 076003 (2008), 0712.0095.
- [14] R. Contino and G. Servant, JHEP **0806**, 026 (2008), 0801.1679.
- [15] J. Aguilar-Saavedra, JHEP **0911**, 030 (2009), 0907.3155.
- [16] J. Mrazek and A. Wulzer, Phys.Rev. **D81**, 075006 (2010), 0909.3977.
- [17] A. De Simone, O. Matsedonskyi, R. Rattazzi, and A. Wulzer, JHEP **1304**, 004 (2013), 1211.5663.
- [18] N. Vignaroli, Phys.Rev. **D86**, 075017 (2012), 1207.0830.
- [19] R. Barcelo, A. Carmona, M. Chala, M. Masip, and J. Santiago, Nucl.Phys. **B857**, 172 (2012), 1110.5914.

- [20] C. Bini, R. Contino, and N. Vignaroli, *JHEP* **1201**, 157 (2012), 1110.6058.
- [21] A. Carmona, M. Chala, and J. Santiago, *JHEP* **1207**, 049 (2012), 1205.2378.
- [22] D. B. Kaplan, *Nucl.Phys.* **B365**, 259 (1991).
- [23] R. Contino, T. Kramer, M. Son, and R. Sundrum, *JHEP* **0705**, 074 (2007), hep-ph/0612180.
- [24] M. Chala and J. Santiago (2013), 1303.0989.
- [25] J. L. Diaz-Cruz, H.-J. He, T. M. Tait, and C. Yuan, *Phys.Rev.Lett.* **80**, 4641 (1998), hep-ph/9802294.
- [26] J. Dai, J. Gunion, and R. Vega, *Phys.Lett.* **B345**, 29 (1995), hep-ph/9403362.
- [27] C. Balazs, J. Diaz-Cruz, H. He, T. M. Tait, and C. Yuan, *Phys.Rev.* **D59**, 055016 (1999), hep-ph/9807349.
- [28] M. S. Carena, S. Mrenna, and C. Wagner, *Phys.Rev.* **D60**, 075010 (1999), hep-ph/9808312.
- [29] B. Gripaios, A. Pomarol, F. Riva, and J. Serra, *JHEP* **0904**, 070 (2009), 0902.1483.
- [30] J. Mrazek, A. Pomarol, R. Rattazzi, M. Redi, J. Serra, et al., *Nucl.Phys.* **B853**, 1 (2011), 1105.5403.
- [31] M. Frigerio, A. Pomarol, F. Riva, and A. Urbano (2012), 1204.2808.
- [32] E. Bertuzzo, T. S. Ray, H. de Sandes, and C. A. Savoy (2012), 1206.2623.
- [33] M. Chala, *JHEP* **1301**, 122 (2013), 1210.6208.
- [34] L. Vecchi (2013), 1304.4579.
- [35] K. Agashe, R. Contino, L. Da Rold, and A. Pomarol, *Phys.Lett.* **B641**, 62 (2006), hep-ph/0605341.
- [36] R. Contino, L. Da Rold, and A. Pomarol, *Phys.Rev.* **D75**, 055014 (2007), hep-ph/0612048.
- [37] G. Panico and A. Wulzer, *JHEP* **1109**, 135 (2011), 1106.2719.
- [38] S. De Curtis, M. Redi, and A. Tesi, *JHEP* **1204**, 042 (2012), 1110.1613.
- [39] A. Abdesselam, E. B. Kuutmann, U. Bitenc, G. Brooijmans, J. Butterworth, et al., *Eur.Phys.J.* **C71**, 1661 (2011), 1012.5412.

- [40] A. Altheimer, S. Arora, L. Asquith, G. Brooijmans, J. Butterworth, et al., *J.Phys.* **G39**, 063001 (2012), 1201.0008.
- [41] J. Alwall, P. Demin, S. de Visscher, R. Frederix, M. Herquet, et al., *JHEP* **0709**, 028 (2007), 0706.2334.
- [42] M. L. Mangano, M. Moretti, F. Piccinini, R. Pittau, and A. D. Polosa, *JHEP* **0307**, 001 (2003), hep-ph/0206293.
- [43] J. Pumplin, D. Stump, J. Huston, H. Lai, P. M. Nadolsky, et al., *JHEP* **0207**, 012 (2002), hep-ph/0201195.
- [44] T. Sjostrand, S. Mrenna, and P. Z. Skands, *JHEP* **0605**, 026 (2006), hep-ph/0603175.
- [45] S. Ovnyn, X. Rouby, and V. Lemaitre (2009), 0903.2225.
- [46] N. Greiner, A. Guffanti, J.-P. Guillet, T. Reiter, and J. Reuter, *PoS DIS2010*, 156 (2010), 1006.5339.
- [47] G. Bevilacqua, M. Czakon, M. Krmer, M. Kubocz, and M. Worek (2013), 1304.6860.
- [48] S. Chatrchyan et al. (CMS Collaboration) (2013), 1303.2985.
- [49] Tech. Rep. CMS-PAS-SUS-12-024, CERN, Geneva (2013).
- [50] G. Cowan, *SigCalc*, a program for calculating discovery significance using profile like-likelihood, available from www.pp.rhul.ac.uk/~cowan/stat/SigCalc/ (2011).
- [51] O. Domenech, A. Pomarol, and J. Serra, *Phys.Rev.* **D85**, 074030 (2012), 1201.6510.
- [52] N. Vignaroli (2011), 1112.0218.
- [53] A. Atre, M. Carena, T. Han, and J. Santiago, *Phys.Rev.* **D79**, 054018 (2009), 0806.3966.
- [54] F. del Aguila, A. Carmona, and J. Santiago, *Phys.Lett.* **B695**, 449 (2011), 1007.4206.
- [55] A. Atre, G. Azuelos, M. Carena, T. Han, E. Ozcan, et al., *JHEP* **1108**, 080 (2011), 1102.1987.
- [56] A. Atre, M. Chala, and J. Santiago (2013), 1302.0270.